

Synthesis and X-ray crystal structures of iron(II) and manganese(II) complexes of unsubstituted and benzyl substituted cross-bridged tetraazamacrocycles

Timothy J. Hubin^{a,*}, James M. McCormick^{a,1}, Simon R. Collinson^{a,2},
Nathaniel W. Alcock^b, Howard J. Clase^b, Daryle H. Busch^a

^a Chemistry Department, The University of Kansas, Lawrence, KS 66045, USA

^b Chemistry Department, The University of Warwick, Coventry CV4 7AL, UK

Received 20 June 2002; accepted 12 August 2002

Abstract

The Mn^{2+} and Fe^{2+} complexes of the cross-bridged tetraazamacrocyclic ligands, 4,11-dibenzyl-1,4,8,11-tetraazabicyclo[6.6.2]hexadecane (**1**), 4,10-dibenzyl-1,4,7,10-tetraazabicyclo[5.5.2]tetradecane (**2**), 1,4,8,11-tetraazabicyclo[6.6.2]hexadecane (**3**), and 1,4,7,10-tetraazabicyclo[5.5.2]tetradecane (**4**) provide new compounds of these elements for fundamental studies and applications. These unsubstituted and benzyl substituted derivatives were prepared for comparison of their structures and properties with the known catalytically active dimethyl cross-bridged ligand complexes, which are especially notable for their exceptional kinetic stabilities and redox activity. The X-ray crystal structures of five complexes demonstrate that the ligands enforce a distorted octahedral geometry on the metals with two *cis* sites occupied by labile ligands. The Fe^{2+} complexes of the unsubstituted ligands form μ -oxo dimers upon exposure to air, which have also been structurally characterized. Cyclic voltammetry of the monomeric complexes shows reversible redox processes for the M^{3+}/M^{2+} couples, which are sensitive to solvent, ring size, and ring substitution.

© 2002 Elsevier Science B.V. All rights reserved.

Keywords: Tetraazamacrocycle; Cross-bridged macrocycle; Macrobicyclic; Iron complexes; Manganese complexes

1. Introduction

Functional catalysts based on manganese and iron complexes of common ligands such as polyamines and polyethers often have limited utility, especially in aqueous media, because of the thermodynamic sink represented by the mineral forms of these elements [1]. Yet, in nature, manganese and iron are ubiquitous in redox related functions. Cytochrome P450 [2], catechol dioxy-

genase [3], methane monooxygenase [4], and lipooxygenase [5] display the power and selectivity found in natural iron-based systems, while Mn catalase [6], mitochondrial superoxide dismutase [7] and Photosystem II [8] similarly illustrate the effectiveness of manganese derivatives. Manganese and iron complexes of *N,N,N'*-trimethyl-1,4,7-triazacyclononane, $Me_3[9]aneN_3$, provides examples in which some solubility is maintained and the manganese complex is a useful oxidation catalyst [9]. However, this and other significant catalysts having in common nitrogen donors and vacant coordination sites, tend to form dimers in which higher valent metal ions are present. Achieving resistance towards oxidative hydrolysis, but doing so with monomeric complexes, is the primary goal of the present work.

The principles of modern coordination chemistry [10] should allow us to design ligands whose complexes are resistant to oxidative hydrolysis while still having

* Corresponding author. Present address: Department of Natural Science, McPherson College, 1600 E. Euclid, P.O. Box 1402, McPherson, KS 67460, USA. Tel.: +1-620-241 0731x1795; fax: +1-503-212 5746.

E-mail address: hubint@mcpherson.edu (T.J. Hubin).

¹ Present address: Division of Science, Truman State, University, Kirksville, MO 63501, USA.

² Present address: Department of Inorganic Chemistry, University of Nottingham, University Park, Nottingham NG7 2RD, UK.

available sites for direct binding of the metal ion to either or both of a terminal oxidant and/or substrate. We envisioned kinetically stable, mononuclear manganese and iron complexes that were not coordinatively saturated by their stabilizing ligand and were capable of supporting higher valent metal ions as well. Specific organic molecules have been identified that should possess the sought-after ligand properties, ethylene cross-bridged tetraazamacrocycles (Fig. 1, Structures 1–6) [11]. These tetradentate ligands are as topologically constrained as the macrobicyclic cryptates, and therefore their complexes should have the kinetic and thermodynamic stabilities associated with this constrained topology. But, in contrast to the prototypical hexadentate cryptate, these ligands should leave labile coordination sites on the metal ion for further reaction. Although previously synthesized in other laboratories [11], these molecules have not been fully exploited as transition metal ligands. We suspected that the great rigidity of these short cross-bridged ligands should impart enormous kinetic stability to their complexes [10], and we have recently shown this to be the case for copper(II) [12] and manganese(II) [13]. This kinetic stability confers great promise in such applications as homogeneous catalysis, where complex stability is a problem.

We have described elsewhere [13] the synthesis and characterization of Fe^{2+} and Mn^{2+} complexes of the methyl-substituted ligands (5 and 6, Fig. 1), and their one-electron oxidized analogues [14]. These compounds have exciting properties such as remarkable stabilities in harsh aqueous conditions and easily accessible higher oxidation states that suggest useful applications as aqueous oxidation catalysts and making them of significant technological interest [15]. Below, we describe the synthesis, X-ray crystal structures and electrochemical behavior of similar complexes where the ligands have been slightly altered to probe the effect on the metal center. Ligands having benzyl groups or simple hydrogens (unsubstituted ligands) as the two nitrogen substituents [16] were combined with the metal ions of interest. We here present the characterization of these

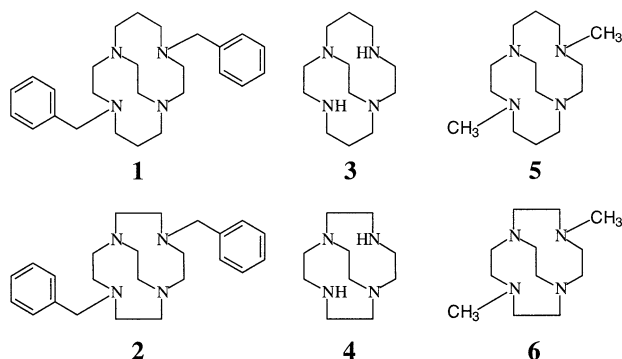


Fig. 1. Cross-bridged ligands [11,15] used in this work.

new complexes and compare them to the methyl-substituted parent ligand complexes.

2. Experimental

N,N-Bis(aminopropyl)ethylenediamine (98%) was purchased from Acros Organics. Glyoxal (40 wt.% in water), benzyl bromide (99%), and sodium borohydride (98%) were purchased from Aldrich Chemical Co. Cyclen was generously supplied by Dow Chemical Co. All solvents were of reagent grade and were dried, when necessary, by accepted procedures [17].

Elemental analyses were performed by the Analytical Service of the University of Kansas or Desert Analytics. Mass spectra were measured by the Analytical Service of the University of Kansas on a VG ZAB HS spectrometer equipped with a xenon gun. Matrices used include NBA (nitrobenzyl alcohol) and TG/G (thioglycerol-glycerol). NMR spectra were obtained on a Bruker AM-500 spectrometer.

2.1. Synthesis

The ligands 4,11-dibenzyl-1,4,8,11-tetraazabicyclo[6.6.2]hexadecane (1), and 1,4,8,11-tetraazabicyclo[6.6.2]hexadecane (3), were prepared according to literature procedures [16] from cyclam, which was made from *N,N*-bis(aminopropyl)ethylenediamine using a modified literature procedure [18]. 4,10-Dibenzyl-1,4,7,10-tetraazabicyclo[5.5.2]tetradecane (2), and 1,4,7,10-tetraazabicyclo[5.5.2]tetradecane (4), were prepared in an analogous manner from cyclen following the Weisman synthesis [16].

2.1.1. $\text{Mn}(\text{I})(\text{CF}_3\text{SO}_3)_2$

In an inert atmosphere glovebox, manganese(II) trifluoromethanesulfonate (approximately 1 mmol) was prepared in situ from manganese metal and trifluoromethanesulfonic acid in MeCN, according to a literature procedure [19], and any excess acid was neutralized by the addition of 1 ml of Et_3N . The ligand 1 (0.406 g, 1 mmol) was dissolved in 6 ml of dry Et_3N in a 25 ml Erlenmeyer flask. The Mn^{2+} solution was added to the stirring ligand solution causing an immediate precipitation of a white powder. The reaction was allowed to stir at 50 °C for 5 more hours, before the precipitate was collected by filtration and washed sparingly with MeCN. Drying in vacuo yielded 0.546 g (72%) of the analytically pure product. *Anal.* Calc. for $\text{C}_{28}\text{H}_{38}\text{F}_6\text{MnN}_4\text{O}_6\text{S}_2$: C, 44.27; H, 5.04; N, 7.38. Found: C, 44.50; H, 5.15; N, 7.48%. The FAB^+ mass spectrum in MeCN (NBA matrix) exhibited peaks at $m/z = 610$ ($\text{Mn}(\text{I})(\text{CF}_3\text{SO}_3)^+$) and 759 ($\text{Mn}(\text{I})(\text{CF}_3\text{SO}_3)_2^+$). Crystals suitable for X-ray diffraction were grown from warm Py.

2.1.2. $MLCl_2$ ($M = Mn^{2+}, Fe^{2+}$; $L = 1, 2$)

The ligand (1 mmol) was dissolved in 10 ml of dry Et_3N in a 25 ml Erlenmeyer flask in an inert atmosphere glovebox. A suspension of 1 mmol of $M(py)_2Cl_2$ ($M = Fe^{2+}, Mn^{2+}$), synthesized by literature procedures [20], in 10 ml of MeCN, was added to the stirring ligand solution. The reaction mixture was stirred for 5 h at 50 °C, during which time the metal salt dissolved and pale brown (Fe^{2+}) or white (Mn^{2+}) finely divided solids precipitated. After cooling, the reaction mixtures were filtered and the solid products were washed sparingly with MeCN and dried in vacuo. Yield: 58–86%. $Fe(1)Cl_2 \cdot 0.5H_2O$: *Anal.* Calc. for $C_{26}H_{39}Cl_2FeN_4O_{0.5}$: C, 57.58; H, 7.25; N, 10.33. Found: C, 57.70; H, 7.20; N, 10.18%. $Mn(1)Cl_2 \cdot 0.5H_2O$: *Anal.* Calc. for $C_{26}H_{39}Cl_2MnN_4O_{0.5}$: C, 57.67; H, 7.26; N, 10.35. Found: C, 57.86; H, 7.38; N, 10.28%. $Fe(2)Cl_2 \cdot 0.5H_2O$: *Anal.* Calc. for $C_{24}H_{35}FeCl_2N_4O_{0.5}$: C, 56.11; H, 6.86; N, 10.91. Found: C, 56.00; H, 6.70; N, 10.71%. $Mn(2)Cl_2$: *Anal.* Calc. for $C_{24}H_{34}Cl_2MnN_4$: C, 57.15; H, 6.79; N, 11.11. Found: C, 56.99; H, 6.54; N, 10.91%. FAB⁺ mass spectra in MeOH (NBA matrix) exhibited peaks at $m/z = MLCl^+$ and $MLCl_2^+$ for all complexes. X-ray quality crystals of $Fe(2)Cl_2$ and $Mn(2)Cl_2$ were grown by the slow evaporation of 3:1 MeOH–Py solutions.

2.1.3. $M(3)Cl_2$ ($M = Mn^{2+}, Fe^{2+}$)

The ligand **3** (1.00 g, 4.42 mmol) was dissolved in 40 ml of dry DMF in a 50 ml Erlenmeyer flask in an inert atmosphere glovebox. Anhydrous MCl_2 (4.42 mmol, $M = Fe^{2+}, Mn^{2+}$) was added to the stirring ligand solution. The reaction was stirred for 16 h at room temperature (r.t.), during which time the metal salt dissolved and pale brown (Fe^{2+}) or white (Mn^{2+}) finely divided solids precipitated. The cooled reaction mixtures were then filtered and the solid products were washed with ether and dried in vacuo. Yield: 46–63%. $Fe(3)Cl_2 \cdot 0.5DMF$: *Anal.* Calc. for $C_{13.5}H_{29.5}Cl_2FeN_{4.5}O_{0.5}$: C, 41.61; H, 7.63; N, 16.18. Found: C, 41.85; H, 7.28; N, 16.10%. $Mn(3)Cl_2$: *Anal.* Calc. for $C_{12}H_{26}Cl_2MnN_4$: C, 40.92; H, 7.44; N, 15.91. Found: C, 41.08; H, 7.13; N, 15.96%. FAB⁺ mass spectra in water (NBA matrix) exhibited peaks at $m/z = MLCl^+$ and $MLCl_2^+$ for both complexes.

2.1.4. $M(4)Cl_2$ ($M = Mn^{2+}, Fe^{2+}$)

The ligand **4** (1.00 g, 5 mmol) was dissolved in 40 ml of dry DMF in a 50 ml Erlenmeyer flask in an inert atmosphere glovebox. Anhydrous MCl_2 (5 mmol, $M = Fe^{2+}, Mn^{2+}$) was added to the stirring ligand solution. The reaction was stirred for 16 h at r.t., during which time the metal salt dissolved. Pale pink (Fe^{2+}) or white (Mn^{2+}) finely divided solids precipitated. The cooled reaction mixtures were then filtered and the solid product was washed with ether and dried in vacuo.

Yield: 51–77%. $Fe(4)Cl_2$: *Anal.* Calc. for $C_{10}H_{22}Cl_2FeN_4$: C, 36.95; H, 6.82; N, 17.24. Found: C, 37.17; H, 6.60; N, 17.13%. $Mn(4)Cl_2$: *Anal.* Calc. for $C_{10}H_{22}Cl_2MnN_4$: C, 37.05; H, 6.84; N, 17.28. Found: C, 36.94; H, 6.74; N, 17.05%. FAB⁺ mass spectra in water (NBA matrix) exhibited peaks at $m/z = MLCl^+$ and $MLCl_2^+$ for both complexes.

2.1.5. $[Cl(3)Fe(\mu-O)Fe(3)Cl]Cl_2 \cdot 2H_2O$

The DMF filtrate from the preparation of $Fe(3)Cl_2$ (see above) was removed from the glovebox. Water (3 ml) was added to this solution and air was bubbled through it overnight. A deep red–brown solution resulted. The solvent was then removed and the brown residue washed with ether (100 ml) to remove any remaining DMF. The remaining brown powder was dried in vacuo. Yield: 801 mg (48% based on ligand). *Anal.* Calc. for $C_{24}H_{56}Cl_4Fe_2N_8O_3$: C, 38.02; H, 7.44; N, 14.78. Found: C, 38.06; H, 7.09; N, 14.62%. The FAB⁺ mass spectrum in MeOH (NBA) exhibited peaks at $m/z = 317$ ($Fe(3)Cl^+$), 352 ($Fe(3)Cl_2^+$), and 650 ($Cl(3)Fe(\mu-O)Fe(3)Cl^+$). X-ray quality crystals were grown by the slow evaporation of an isopropanol solution and contained three waters of crystallization.

2.1.6. $[Cl(4)Fe(\mu-O)Fe(4)Cl][PF_6]_2$

The DMF filtrate from the preparation of $Fe(4)Cl_2$ (see above) was removed from the glovebox. Water (3 ml) was added to this solution and air was bubbled through it overnight. A deep red–brown solution resulted. The solvent was then removed and the brown residue washed with ether (100 ml) to remove any remaining DMF. The remaining brown powder was dissolved in 30 ml of dry MeOH. One gram of ammonium hexafluorophosphate in 15 ml of dry MeOH was added to the above solution causing a brown precipitate to form. The solid was collected by filtration, washed with MeOH and ether and vacuum dried. Yield: 991 mg (43%). *Anal.* Calc. for $C_{20}H_{44}Cl_2F_{12}Fe_2N_8OP_2$: C, 27.14; H, 5.01; N, 12.66. Found: C, 27.29; H, 4.81; N, 12.38%. The FAB⁺ mass spectrum in DMF (NBA) exhibited a peak at $m/z = 593$ ($Cl(4)Fe(\mu-O)Fe(4)Cl^+$). X-ray quality crystals of the crude dichloride salt prior to ammonium hexafluorophosphate addition, were grown by the slow evaporation of a DMF solution and contained two waters of crystallization.

2.2. Physical methods

Electrochemical experiments were performed on a Princeton Applied Research Model 175 programmer and Model 173 potentiostat in dry CH_3CN using a homemade cell in an inert atmosphere dry box under N_2 . Either a button Pt or a button glassy carbon electrode was used as the working electrode in conjunc-

tion with a Pt-wire counter electrode and a Ag-wire pseudo-reference electrode. Tetrabutylammonium hexafluorophosphate (0.1 M) was the supporting electrolyte in all cases. The measured potentials were referenced to SHE using ferrocene (+0.400 V vs. SHE) as an internal standard.

2.3. Crystal structure analysis

X-ray data were collected with a Siemens SMART three-circle system with CCD area detector using graphite monochromated Mo K α radiation ($\lambda = 0.71073 \text{ \AA}$) [21]. The crystals were held at the specified temperature with the Oxford Cryosystem Cooler [22]. Absorption corrections were applied by the Ψ -scan method, and none of the crystals showed any decay during data collection. Complete crystal data are in Table 1. The structures were solved by direct methods using SHELXS [23] (TREF) with additional light atoms found by Fourier methods. Hydrogen atoms were added at calculated positions and refined using a riding model. Anisotropic displacement parameters were used for all non-H atoms, while H-atoms were given isotropic displacement parameters equal to 1.2 (or 1.5 for methyl hydrogen atoms) times the equivalent isotropic displacement parameter for the atom to which the H-atom is attached. Refinement used SHELXL-96 [24]. Selected bond lengths and angles for the five complexes are in Table 2.

2.3.1. Specific structures

Mn(1)(CF₃SO₃)₂: crystal character: yellow diamond plates. Systematic absences indicated space group *Pbcn*. Mn(2)Cl₂: crystal character: colorless squares. Systematic absences indicated space group *Cc* or *C2/c*; the latter was chosen and shown to be correct by satisfactory refinement. Fe(2)Cl₂: crystal character: pale brown plates. Systematic absences indicated space group *Cc* or *C2/c*; the latter was chosen and shown to be correct by satisfactory refinement. [Cl(3)Fe(μ -O)Fe(3)Cl]Cl₂·3H₂O: crystal character: thin brown plates. Systematic absences indicated space group *P2₁/c*. Three lattice water molecules were located. Although one ligand is very precisely located, it appears that the other (attached to Fe(1)) is partly occupied by the opposite diastereomer. The resulting disorder is visible in the elongated ellipsoids of the ligand atoms, corresponding to the superposition of the two species, and required the inclusion of two additional low occupancy sites (C(12a) and C(17a)). [Cl(4)Fe(μ -O)Fe(4)Cl]Cl₂·2H₂O: crystal character: deep red thin plates. Systematic absences indicated space group *P2₁/c*. Two lattice water molecules were located.

3. Results and discussion

3.1. Preparation of metal complexes

As noted in a previous communication [12], only Cu²⁺ and Ni²⁺, the thermodynamically strongest binding (first row, divalent) transition metal ions [25], had been complexed to ethylene cross-bridged tetraaza-macrocycles prior to our work [16]. Our early attempts at the complexation of **5** and **6** with Fe²⁺ and Mn²⁺ salts in protic solvents or in aprotic solvents using hydrated metal salts were entirely unsuccessful. We therefore soon concluded that Cu²⁺ and Ni²⁺ are much better at competing with protons for the binding cavity in protic solvents than are other divalent transition metal ions. This is especially true of the ions of primary interest here, the relatively hard oxophilic ions of manganese and iron. We attribute this behavior to the proton-sponge nature of the ligands [11], which has been confirmed by titration. We found that in an aqueous medium the diprotonated form of free ligand **5** behaves as a monoprotic weak acid with a pK_{a1} of 9.58(3); stoichiometrically, two H⁺ are bound, demonstrating that pK_{a2} must be substantially greater than 13 [13]. The conclusion is clear, that these ligands bind at least one proton very strongly indeed, and that only the most strongly binding metal ions can compete with that proton for the cavity it occupies.

The obstacle, once identified, was overcome by minimizing the activity of protons in the reaction system. The complexes of a broad array of transition metal ions have been prepared with these ligands through the use of anhydrous metal reagents with strictly deprotonated ligands in rigorously dry, aprotic solvents under a dry, inert atmosphere [12]. The Fe²⁺ and Mn²⁺ complexes with parent ligands **5** and **6** were prepared from the corresponding anhydrous M(py)₂Cl₂ starting material in CH₃CN. Unfortunately, complexation of **1** and **2** via the same reaction was not successful. Possible explanations include decreased solubility of the ligands in acetonitrile, increased steric bulk (the benzyl groups) near the ligand cavity, and/or increased ligand basicity (not measured). Several sets of reaction conditions were investigated until success was achieved in 1:1 triethylamine–acetonitrile solution, from either triflate and dichlorobis-pyridine metal starting materials. Triethylamine is generally used as a mild base in complexation reactions, but was found to be a good solvent for the ligands, which are not readily soluble in many of the aprotic solvents otherwise necessary for complexation of these ligands. Complexation of the unsubstituted ligands **3** and **4** proved less challenging, and followed protocols [13] established with ligands **1** and **2**, except for the substitution of DMF as the solvent.

The air oxidation of the complexes with **3** and **4** have been studied. Experimentally, the Fe²⁺ complexes of

Table 1
Crystal data and structural refinement details

	Mn(1)(CF ₃ SO ₃) ₂	Mn(2)Cl ₂	Fe(2)Cl ₂	[Cl(3)Fe(μ-O)Fe(3)Cl]Cl ₂ ·3H ₂ O	[Cl(4)Fe(μ-O)Fe(4)Cl]Cl ₂ ·2H ₂ O
Empirical formula	C ₂₈ H ₃₈ F ₆ MnN ₄ O ₆ S ₂	C ₂₄ H ₃₄ Cl ₂ MnN ₄	C ₂₄ H ₃₄ Cl ₂ MnN ₄	C ₂₄ H ₅₈ Cl ₄ Fe ₂ N ₈ O ₄	C ₂₀ H ₄₄ Cl ₄ Fe ₂ N ₈ O ₃
Formula weight	759.68	504.39	505.30	776.28	698.13
Temperature (K)	180(2)	293(2)	180(2)	180(2)	180(2)
Crystal system	orthorhombic	monoclinic	monoclinic	monoclinic	monoclinic
Space group	<i>Pbcn</i>	<i>C2/c</i>	<i>C2/c</i>	<i>P2₁/c</i>	<i>P2₁/c</i>
<i>a</i> (Å)	16.004(2)	8.97080(10)	8.9453(4)	14.3930(10)	10.6863(3)
<i>b</i> (Å)	9.71120(10)	13.3513(2)	13.3191(6)	22.6960(10)	17.6254(2)
<i>c</i> (Å)	21.3157(2)	20.02770(10)	19.9448(9)	10.3900(10)	16.4448(2)
β (°)	90	91.4400	91.7100(10)	92.971(5)	108.6220(10)
<i>V</i> (Å ³)	3312.76(5)	2398.00(5)	2375.2(2)	3389.5(4)	2935.22(10)
<i>Z</i>	4	4	4	8	4
ρ_{calc} (g cm ⁻³)	1.523	1.397	1.413	1.308	1.580
Absolute coefficient (cm ⁻¹)	6.05	7.93	8.79	10.46	13.91
Crystal size (mm)	0.80 × 0.45 × 0.20	0.39 × 0.36 × 0.18	0.30 × 0.26 × 0.10	0.55 × 0.10 × 0.02	0.2 × 0.2 × 0.04
Maximum θ (°)	28.57	28.52	28.56	25.00	24.00
Index ranges	-20 ≤ <i>h</i> ≤ 21, -12 ≤ <i>k</i> ≤ 9, -27 ≤ <i>l</i> ≤ 23	-11 ≤ <i>h</i> ≤ 5, -17 ≤ <i>k</i> ≤ 16, -25 ≤ <i>l</i> ≤ 26	-11 ≤ <i>h</i> ≤ 11, -17 ≤ <i>k</i> ≤ 17, -23 ≤ <i>l</i> ≤ 25	-12 ≤ <i>h</i> ≤ 18, -27 ≤ <i>k</i> ≤ 29, -13 ≤ <i>l</i> ≤ 13	-14 ≤ <i>h</i> ≤ 10, -23 ≤ <i>k</i> ≤ 23, -21 ≤ <i>l</i> ≤ 19
Reflections collected	18842	7040	7022	16722	13227
Independent reflections	3971	2766	2797	5918	4607
Observed reflections ^a	3117	2260	2168	3804	2848
Refinement method	full-matrix on <i>F</i> ²	full-matrix on <i>F</i> ²	full-matrix on <i>F</i> ²	full-matrix on <i>F</i> ²	full-matrix on <i>F</i> ²
Data/restraints/parameters	3971/13/251	2766/0/141	2797/0/141	5918/9/419	4607/0/334
Final <i>R</i> indices [<i>I</i> > 2σ(<i>I</i>)]	<i>R</i> ₁ = 0.0471	<i>R</i> ₁ = 0.0294	<i>R</i> ₁ = 0.0339	<i>R</i> ₁ = 0.0608	<i>R</i> ₁ = 0.0619
<i>R</i> indices (all data) ^{b,c}	<i>wR</i> ₂ = 0.1175	<i>wR</i> ₂ = 0.0756	<i>wR</i> ₂ = 0.0820	<i>wR</i> ₂ = 0.1471	<i>wR</i> ₂ = 0.1290
Weight parameters <i>a</i> , <i>b</i>	0.0430, 3.2000	0.0401, 0.2776	0.0431, 0.0000	0.0560, 10.5000	0.0370, 8.2000
Goodness-of-fit on <i>F</i> ²	1.086	1.035	0.985	0.997	1.014
Largest peak/hole (e Å ⁻³)	0.504 and -0.436	0.234 and -0.304	0.313 and -0.328	0.663 and -0.555	0.847 and -0.873

both of these ligands immediately turn from pale yellow to deep red–brown in solution when exposed to air. This behavior does not occur with the Fe²⁺ complexes of ligands **1**, **2**, **5**, or **6**; their solutions only become somewhat darker yellow in color under the same conditions. One possible reaction for **3** and **4** is ligand oxidation, as secondary amines are notoriously easy to oxidize to imines in transition metal complexes [26]. Another possibility is metal ion oxidation and formation of oxide or hydroxide bridged dimers. Cache[®] molecular modeling studies indicated that dimerization of the latter complexes should be sterically inhibited by the N-alkyl groups, which would need to occupy the same space as the second ligand in a typical μ-oxo dimer. However, no such steric problems exist for the unsubstituted ligands **3** and **4**. The products of these reactions

have been structurally characterized (vide infra), showing that these ligand complexes do indeed form μ-oxo Fe³⁺ dimers [27] on oxidation by air.

The manganese(II) complexes with the methyl-substituted ligand **5** has been extensively studied under conditions favorable for dimerization, and no such reaction has yet been observed. In contrast, the Mn²⁺ complex of **4** immediately turns from colorless to deep green upon exposure of a DMF solution to air. In addition to its telling color, the solution has the characteristic 16-line EPR signal, associated with a Mn³⁺/Mn⁴⁺ oxo-bridged dimer [28]. Surprisingly, a solution of the manganese(II) complex of **3** turns a pale red color under the same conditions and lacks the 16-line EPR. Obviously, a different reaction is taking place, although neither of the products from the air

Table 2
Selected bond lengths (Å) and angles (°)

For Mn(1)(CF ₃ SO ₃) ₂			
<i>Bond lengths</i>			
Mn(1)–O(1)#1	2.153(2)	S(1)–O(3)	1.428(2)
Mn(1)–N(4)	2.266(2)	S(1)–O(1)	1.452(2)
Mn(1)–N(1)	2.295(2)	S(1)–Cl6Aa	1.852(12)
S(1)–O(2)	1.424(2)		
<i>Bond angles</i>			
O(1)#1–Mn(1)–O(1)	94.93(9)	N(4)–Mn(1)–N(1)#1	87.58(8)
O(1)–Mn(1)–N(4)	93.11(9)	O(1)–Mn(1)–N(1)	97.26(7)
O(1)–Mn(1)–N(4)#1	170.40(9)	N(4)–Mn(1)–N(1)	81.06(9)
N(4)–Mn(1)–N(4)#1	79.40(14)	N(1)#1–Mn(1)–N(1)	165.25(10)
O(1)–Mn(1)–N(1)#1	92.71(7)		
For Mn(2)Cl ₂			
<i>Bond lengths</i>			
Mn(1)–N(4)	2.3051(13)	Mn(1)–Cl(1)	2.4276(4)
Mn(1)–N(1)	2.3311(12)		
<i>Bond angles</i>			
N(4)–Mn(1)–N(4)#1	74.56(8)	N(4)#1–Mn(1)–Cl(1)	168.60(4)
N(4)–Mn(1)–N(1)#1	77.69(4)	N(1)#1–Mn(1)–Cl(1)	102.55(3)
N(4)#1–Mn(1)–N(1)#1	74.06(4)	N(1)–Mn(1)–Cl(1)	100.84(3)
N(1)#1–Mn(1)–N(1)	144.30(6)	Cl(1)–Mn(1)–Cl(1)#1	97.21(3)
N(4)–Mn(1)–Cl(1)	94.13(4)		
For Fe(2)Cl ₂			
<i>Bond lengths</i>			
Fe(1)–N(4)	2.234(2)	Fe(1)–Cl(1)	2.4004(5)
Fe(1)–N(1)	2.2757(14)		
<i>Bond angles</i>			
N(4)#1–Fe(1)–N(4)	76.92(9)	N(1)–Fe(1)–Cl(1)	99.18(4)
N(4)–Fe(1)–N(1)#1	79.21(5)	N(4)–Fe(1)–Cl(1)#1	171.26(5)
N(4)–Fe(1)–N(1)	75.63(6)	N(1)–Fe(1)–Cl(1)#1	102.61(4)
N(1)#1–Fe(1)–N(1)	147.71(8)	Cl(1)–Fe(1)–Cl(1)#1	94.39(3)
N(4)–Fe(1)–Cl(1)	94.35(5)		
For [Cl(3)Fe(μ-O)Fe(3)Cl]Cl ₂ ·3H ₂ O			
<i>Bond lengths</i>			
Fe(1)–O(1)	1.831(4)	O(1)–Fe(2)	1.820(4)
Fe(1)–N(111)	2.145(5)	Fe(2)–N(211)	2.157(5)
Fe(1)–N(14)	2.157(5)	Fe(2)–N(24)	2.152(5)
Fe(1)–N(11)	2.180(5)	Fe(2)–N(28)	2.207(5)
Fe(1)–N(18)	2.283(6)	Fe(2)–N(21)	2.287(5)
Fe(1)–Cl(1)	2.368(2)	Fe(2)–Cl(2)	2.350(2)
<i>Bond angles</i>			
O(1)–Fe(1)–N(111)	95.2(2)	O(1)–Fe(2)–N(211)	94.9(2)
O(1)–Fe(1)–N(14)	98.6(2)	O(1)–Fe(2)–N(24)	101.5(2)
N(111)–Fe(1)–N(14)	163.6(2)	N(211)–Fe(2)–N(24)	159.6(2)
O(1)–Fe(1)–N(11)	95.4(2)	O(1)–Fe(2)–N(28)	94.9(2)
N(111)–Fe(1)–N(11)	88.3(2)	N(211)–Fe(2)–N(28)	81.6(2)
N(14)–Fe(1)–N(11)	81.8(2)	N(24)–Fe(2)–N(28)	85.1(2)
O(1)–Fe(1)–N(18)	171.8(2)	O(1)–Fe(2)–N(21)	173.9(2)
N(111)–Fe(1)–N(18)	79.3(2)	N(211)–Fe(2)–N(21)	82.7(2)
N(14)–Fe(1)–N(18)	85.9(2)	N(24)–Fe(2)–N(21)	79.7(2)
N(11)–Fe(1)–N(18)	78.5(2)	N(28)–Fe(2)–N(21)	79.2(2)
O(1)–Fe(1)–Cl(1)	98.50(12)	O(1)–Fe(2)–Cl(2)	98.42(13)
N(111)–Fe(1)–Cl(1)	93.96(14)	N(211)–Fe(2)–Cl(2)	97.56(14)
N(14)–Fe(1)–Cl(1)	92.6(2)	N(24)–Fe(2)–Cl(2)	91.83(13)
N(11)–Fe(1)–Cl(1)	165.7(2)	N(28)–Fe(2)–Cl(2)	166.63(13)
N(18)–Fe(1)–Cl(1)	88.03(14)	N(21)–Fe(2)–Cl(2)	87.42(13)
Fe(2)–O(1)–Fe(1)	144.1(2)		

Table 2 (Continued)

For [Cl(4)Fe(μ -O)Fe(4)Cl]Cl₂·2H₂O*Bond lengths*

Fe(1)–O(1)	1.818(4)	Fe(2)–O(1)	1.807(4)
Fe(1)–N(14)	2.149(6)	Fe(2)–N(210)	2.174(5)
Fe(1)–N(110)	2.160(5)	Fe(2)–N(24)	2.188(5)
Fe(1)–N(11)	2.173(5)	Fe(2)–N(21)	2.198(5)
Fe(1)–N(17)	2.257(5)	Fe(2)–N(27)	2.266(5)
Fe(1)–Cl(11)	2.349(2)	Fe(2)–Cl(21)	2.354(2)

Bond angles

O(1)–Fe(1)–N(14)	101.2(2)	O(1)–Fe(2)–N(24)	103.2(2)
O(1)–Fe(1)–N(110)	103.1(2)	N(210)–Fe(2)–N(24)	146.8(2)
N(14)–Fe(1)–N(110)	148.3(2)	O(1)–Fe(2)–N(21)	94.9(2)
O(1)–Fe(1)–N(11)	96.3(2)	N(210)–Fe(2)–N(21)	79.9(2)
N(14)–Fe(1)–N(11)	78.7(2)	N(24)–Fe(2)–N(21)	76.1(2)
N(110)–Fe(1)–N(11)	78.7(2)	O(1)–Fe(2)–N(27)	172.1(2)
O(1)–Fe(1)–N(17)	174.0(2)	N(210)–Fe(2)–N(27)	74.6(2)
N(14)–Fe(1)–N(17)	77.2(2)	N(24)–Fe(2)–N(27)	78.1(2)
N(110)–Fe(1)–N(17)	76.4(2)	N(21)–Fe(2)–N(27)	77.7(2)
N(11)–Fe(1)–N(17)	77.7(2)	O(1)–Fe(2)–Cl(21)	97.82(14)
O(1)–Fe(1)–Cl(11)	98.02(14)	N(210)–Fe(2)–Cl(21)	98.6(2)
N(14)–Fe(1)–Cl(11)	99.1(2)	N(24)–Fe(2)–Cl(21)	99.83(14)
N(110)–Fe(1)–Cl(11)	97.3(2)	N(21)–Fe(2)–Cl(21)	167.23(14)
N(11)–Fe(1)–Cl(11)	165.6(2)	N(27)–Fe(2)–Cl(21)	89.62(14)
N(17)–Fe(1)–Cl(11)	87.95(14)	Fe(2)–O(1)–Fe(1)	178.9(3)
O(1)–Fe(2)–N(210)	101.4(2)		

oxidation of these Mn²⁺ precursors has been satisfactorily characterized. The cause of this difference in behavior is unlikely to be steric, since the iron complex of this ligand can dimerize on air oxidation.

3.1.1. Crystal structures

X-ray crystal structures for three monomeric complexes all with dibenzyl ligands, are shown in Fig. 2. These structures confirm the expected geometric properties of the cross-bridged ligands, which are constrained by the short cross-bridge to folded conformations. In all three cases, the macrobicycle occupies two axial and two *cis* equatorial sites of distorted octahedra, while the remaining *cis* equatorial sites are occupied by either two triflate ligands or two chloride ligands. In the chemistry of the unbridged parent macrocycles, with few exceptions [27], 1,4,8,11-tetraazacycotetradecane, or *cyclam*, binds metal ions in a square planar fashion [28], occupying all four equatorial sites of octahedral complexes, which locates the two labile ligand binding sites at the *trans*, axial positions. Cyclen is too small to fit completely around the metal ion, and generally folds to occupy two *cis* equatorial and the two axial sites of octahedral metal ions [29], a strict parallel to the coordination reported here for **1** and **2**. The short cross-bridge of **1** forces the cyclam ring system to behave more like cyclen. The consequences that two *cis* labile sites have on the reactivity of these complexes are currently being explored [13,15].

A more detailed inspection of the three structures reveals several interesting trends. First, the size of the ring system dictates the distortion of the octahedra. The

14-membered ring in **1** engulfs the metal ion more fully than does the 12-membered ring in **2**. The N_{ax}–M–N_{ax} bond angle for Mn(**1**)(CF₃SO₃)₂ is 165.25(10)°, while for Mn(**2**)Cl₂, it is only 144.30(6)°. Likewise, the N_{eq}–M–N_{eq} angles are 79.40(14) and 74.56(8)° for Mn(**1**)(CF₃SO₃)₂ and Mn(**2**)Cl₂, respectively. The smaller angles for the smaller macrobicycle demonstrate how the metal ion is less engulfed in the ligand cavity. Surprisingly, the triflate complex of **1** contains a Mn²⁺ ion deeper in the ligand cleft than in the related dichloro complex of **5** [13]. In this structure, Mn(**5**)Cl₂, the N_{ax}–M–N_{ax} and N_{eq}–M–N_{eq} bond angles are 158.0(2) and 75.6(2)°, respectively, several degrees smaller than in Mn(**1**)(CF₃SO₃)₂. It might be expected that the more bulky triflate ligands in the complex of **1** would draw the Mn²⁺ ion further out of the ligand cleft than the chloride atoms in the complex of **5**. Since the benzyl groups are extended axially, it appears that they leave sufficient equatorial space to accommodate the two triflate ligands without costly steric interactions. It then becomes logical that the smaller triflate oxygen atoms bound to Mn²⁺ allow this ion to move deeper into the ligand cavity than the larger chloro ligands. Electronic factors might also contribute; the poorly complementary triflate ligands do not add enough electron density, so the metal ion has to delve deeper into the tetradentate ligand cavity. These postulated steric effects also explain the larger Cl–Mn–Cl angle (98.85(6)°) in Mn(**5**)Cl₂, versus that of the O–Mn–O angle (94.93(9)°) in Mn(**1**)(CF₃SO₃)₂.

A second observation is that the smaller Fe²⁺ ion is more fully engulfed by macrobicycle **2** than is the larger

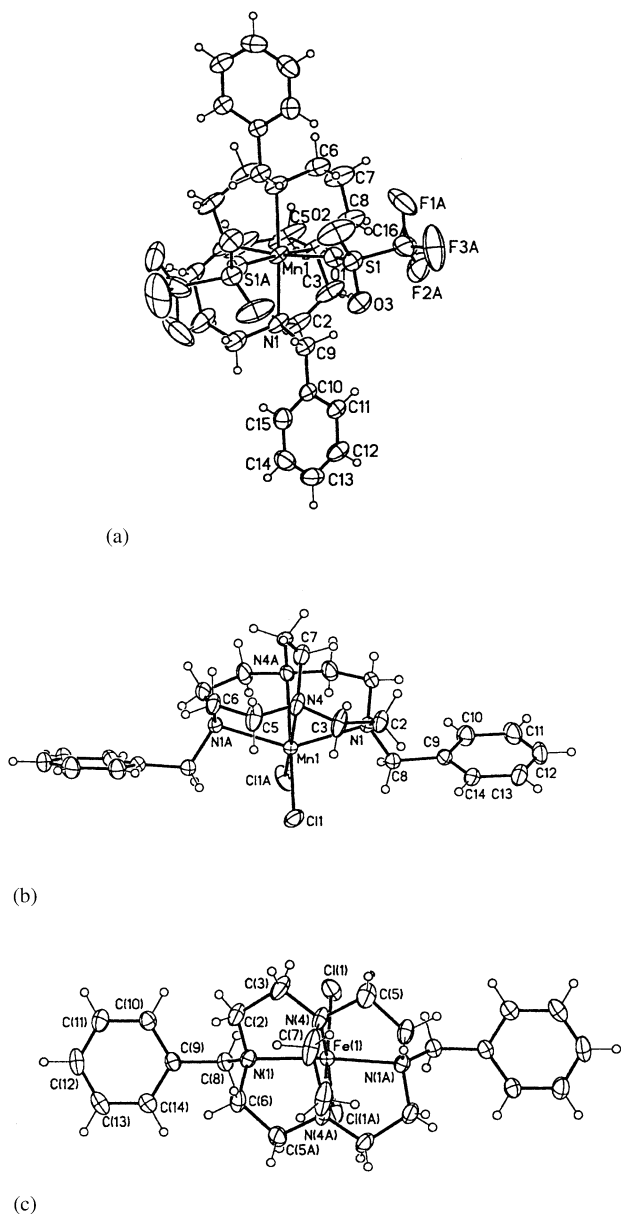


Fig. 2. Views of the crystal structures of: (a) $\text{Mn(1)(CF}_3\text{SO}_3)_2$; (b) Mn(2)Cl_2 ; and (c) Fe(2)Cl_2 .

Mn^{2+} ion. $\text{N}_{\text{ax}}\text{-M-N}_{\text{ax}}$ is $147.71(8)^\circ$ for Fe(2)Cl_2 , $144.30(6)^\circ$ for Mn(2)Cl_2 . The $\text{N}_{\text{eq}}\text{-M-N}_{\text{eq}}$ angles are $76.92(9)$ and $74.56(8)^\circ$ for Fe(2)Cl_2 and Mn(2)Cl_2 , respectively. In these two complexes, the average Fe-N distance is 2.255 \AA , while the average Mn-N distance is 2.318 \AA , confirming the size relationship of the Fe^{2+} and Mn^{2+} cations. These effects of macrocycle ring size and metal ionic radius, influence how deep the metal ion resides within the ligand cavity and determine how close the coordination geometry is to a true octahedron; they have been consistently observed with several different metal ions and ligand ring sizes [13,14].

The intermolecular interactions of the two ligand **2** complexes in the solid state should also be noted. The

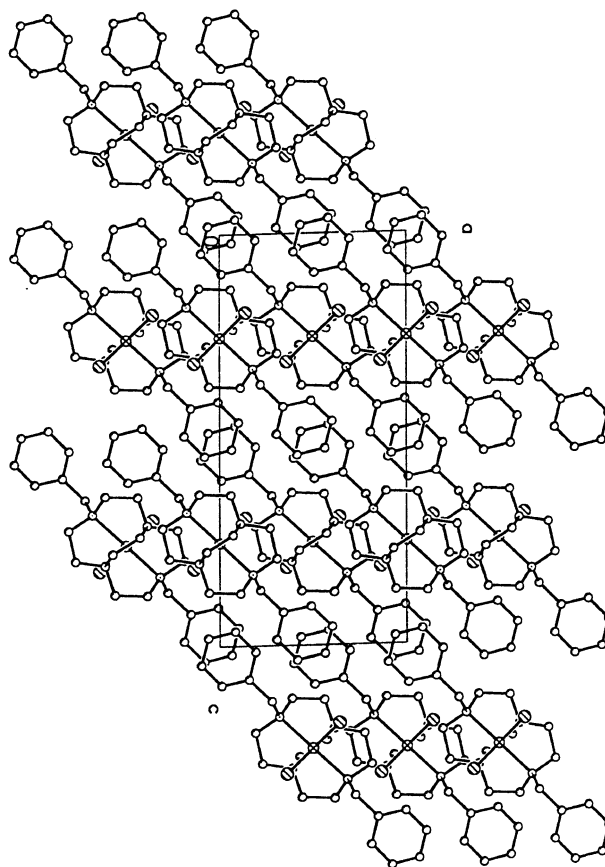


Fig. 3. The crystal packing diagram of Fe(2)Cl_2 showing the $\pi\text{-}\pi$ stacking interactions between benzyl groups of neighboring molecules.

benzyl groups extending from the macrobicyclic complexes make classical $\pi\text{-}\pi$ interactions with benzyl groups from neighboring molecules, as demonstrated in the crystal packing diagram of Fe(2)Cl_2 (Fig. 3). The two benzyl groups are in the slipped arrangement where one aromatic carbon is directly above the centroid of its partners aromatic ring [30]. The paired benzyl groups are 3.32 \AA apart, also a normal distance for this type of interaction [30]. The strengths of these interactions in the solid state may contribute to the general low solubilities of the complexes of ligands **1** and **2**.

The crystal structures of the dimeric iron(III) complexes of ligands **3** and **4** are represented in Fig. 4. The Fe^{3+} ions of these complexes are again found in pseudo-octahedral, six-coordinate geometries, similar to most monomeric complexes of the methyl- and benzyl substituted ligands [13,14]. Commonly, such dimers have a coordination number of 5, although six- and seven-coordinate dimers are known [27]. It is interesting that the monodentate chloro ligands are maintained in the present structures, but since the macrobicyclic ligands are uncharged, the only Coulombic forces influencing the monoanionic halide are attractive. Also, the folded ligand conformations help separate the ligands from each other, easing the steric interactions that might

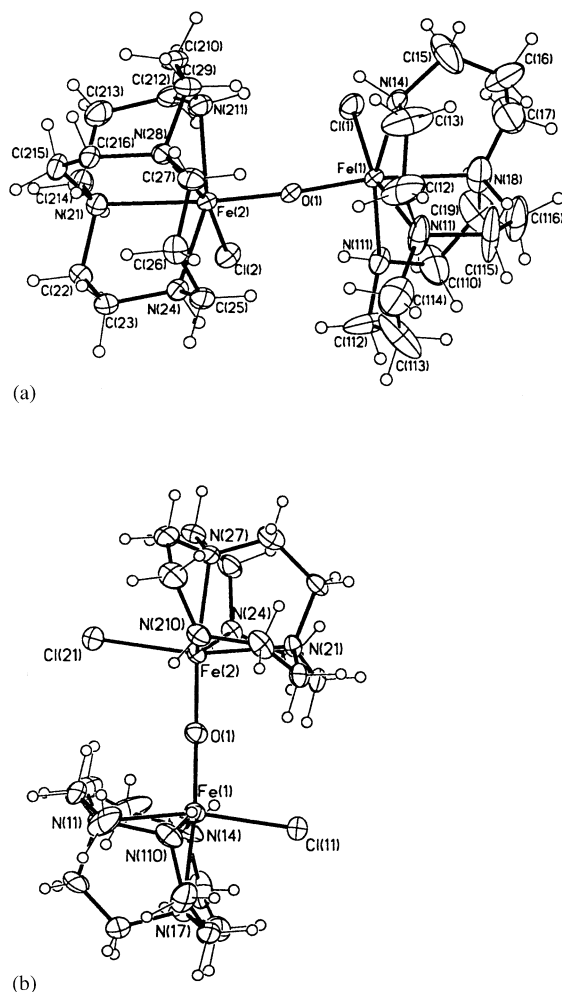


Fig. 4. Views of the crystal structures of: (a) $[\text{Cl}(3)\text{Fe}(\mu\text{-O})\text{Fe}(3)\text{Cl}]\text{Cl}_2 \cdot 3\text{H}_2\text{O}$; and (b) $[\text{Cl}(4)\text{Fe}(\mu\text{-O})\text{Fe}(4)\text{Cl}]\text{Cl}_2 \cdot 2\text{H}_2\text{O}$.

favor lower coordination numbers with more nearly planar ligands. In the ligands, all of the C–N bond lengths are within the accepted values for single bonds, confirming the absence of ligand oxidation during the formation of the dimers [31]. In contrast, such ligand oxidation is common in Fe^{2+} complexes of secondary amine-containing macrocycles [26]. As expected, the bond distances between the donor nitrogens are shorter for these Fe^{3+} complexes than for similar Fe^{2+} complexes. For example, in the Fe^{2+} complexes of **5** and **6**, the Fe–N(3°) bond distances average 2.27 (L = **5**) and 2.26 Å (L = **6**), while for **1** and **2**, the average Fe–N(3°) are 2.24 (L = **1**) and 2.22 Å (L = **2**). The secondary amine– Fe^{3+} bond lengths are somewhat shorter: Fe–N(2°) averages 2.15 Å for L = **1** and 2.17 Å for L = **2**. Even more affected by the change in metal oxidation state are the Fe–Cl bond distances: 2.43 Å for $\text{Fe}(\mathbf{5})\text{Cl}_2$, 2.41 Å for $\text{Fe}(\mathbf{6})\text{Cl}_2$, 2.36 Å for the dimer of **1**, and 2.35 Å for the dimer of **2** (averages). The Fe–O bond distances are in the range expected for dimers of this

type [27], averaging 1.83 Å for the dimer of **1** and 1.81 Å for the dimer of **2**.

Perhaps most interesting is the degree of linearity in the Fe–O–Fe bond angles. For the ligand **2** dimer, this angle is almost completely linear, with a value of $178.9(3)^\circ$. In contrast, the Fe–O–Fe angle in the ligand **1** dimer is only $144.1(2)^\circ$. These values approach the extremes for linearity and non-linearity, respectively, for μ -oxo bridged iron(III) dimers [25]. A possible rationalization of this observation is that the bonding in **4** is compromised by poor complementarity (the small ligand size). This dimensional relationship decreases the N–Fe–N bond angles, which in turn reduces orbital overlap.

The trend in the ability of the ligands to enclose the metal ion is unaffected by absence of N-substitution. The ligand **3** dimer has an average $\text{N}_{\text{ax}}\text{-M-N}_{\text{ax}}$ angle of 161.60° , while this angle averages 147.55° for the ligand **4** dimer. The $\text{N}_{\text{eq}}\text{-M-N}_{\text{eq}}$ angles average 78.85 and 77.70° for the ligand **3** dimer and the ligand **4** dimer, respectively.

3.1.2. Electrochemistry

Electrochemical studies were used to compare the monomeric complexes of the benzyl-substituted ligands **1** and **2** and the unsubstituted ligands **3** and **4** with the methyl-substituted ligand **5** and **6** complexes, whose previous characterization gave promise of oxidative catalytic behavior in aqueous media [13–15]. The new complexes provide the opportunity to probe the effect of the N-substituents on the accessibility of higher metal oxidation states. The cyclic voltammograms of the complexes were obtained in either acetonitrile or DMF in an inert atmosphere glovebox. The redox potentials and peak separations are shown in Table 3. These rigid ligands stabilize a range of oxidation states for manganese in acetonitrile, from Mn^{2+} to Mn^{4+} as shown by

Table 3
Redox potentials (vs. SHE) for the complexes with peak separations

Complex	Solvent	Redox couple	$E_{1/2}$ (V)	$(E_a - E_c)$ (mV)
$\text{Mn}(\mathbf{5})\text{Cl}_2$	MeCN	$\text{Mn}^{3+}/\text{Mn}^{2+}$	+0.585	61
		$\text{Mn}^{4+}/\text{Mn}^{3+}$	+1.343	65
$\text{Mn}(\mathbf{6})\text{Cl}_2$	MeCN	$\text{Mn}^{3+}/\text{Mn}^{2+}$	+0.466	70
		$\text{Mn}^{4+}/\text{Mn}^{3+}$	+1.232	102
$\text{Mn}(\mathbf{5})\text{Cl}_2$	DMF	$\text{Mn}^{3+}/\text{Mn}^{2+}$	+0.522	67
$\text{Mn}(\mathbf{1})\text{Cl}_2$	DMF	$\text{Mn}^{3+}/\text{Mn}^{2+}$	+0.577	72
$\text{Mn}(\mathbf{2})\text{Cl}_2$	DMF	$\text{Mn}^{3+}/\text{Mn}^{2+}$	+0.400	65
$\text{Mn}(\mathbf{3})\text{Cl}_2$	DMF	$\text{Mn}^{3+}/\text{Mn}^{2+}$	+0.239	79
$\text{Mn}(\mathbf{4})\text{Cl}_2$	DMF	$\text{Mn}^{3+}/\text{Mn}^{2+}$	+0.389	280
$\text{Fe}(\mathbf{5})\text{Cl}_2$	MeCN	$\text{Fe}^{3+}/\text{Fe}^{2+}$	+0.110	63
$\text{Fe}(\mathbf{6})\text{Cl}_2$	MeCN	$\text{Fe}^{3+}/\text{Fe}^{2+}$	+0.036	64
$\text{Fe}(\mathbf{1})\text{Cl}_2$	DMF	$\text{Fe}^{3+}/\text{Fe}^{2+}$	+0.157	85
$\text{Fe}(\mathbf{2})\text{Cl}_2$	DMF	$\text{Fe}^{3+}/\text{Fe}^{2+}$	+0.071	85
$\text{Fe}(\mathbf{3})\text{Cl}_2$	DMF	$\text{Fe}^{3+}/\text{Fe}^{2+}$	–0.113	78
$\text{Fe}(\mathbf{4})\text{Cl}_2$	DMF	$\text{Fe}^{3+}/\text{Fe}^{2+}$	–0.055	89

the two reversible oxidations of Mn(5)Cl₂ and Mn(6)Cl₂. In contrast, only the Fe³⁺/Fe²⁺ couple is observed for Fe(5)Cl₂ and Fe(6)Cl₂ in acetonitrile. Unfortunately, the complexes of ligands 1–4 are not sufficiently soluble in acetonitrile to permit electrochemical studies in that medium. But, these complexes do have good solubility in DMF, and their cyclic voltammograms were obtained in this solvent. The complex Mn(5)Cl₂ was examined in both solvents as a test for the effect of solvent on the redox potentials. This complex only exhibits one reversible oxidation in DMF, because the solvent itself is oxidized at potentials corresponding to the Mn⁴⁺/Mn³⁺ couple. The Mn³⁺/Mn²⁺ couple is observed in both solvents with only small changes in potential or reversibility: +0.585 V (61 mV) in MeCN versus +0.522 V (67 mV) in DMF.

Comparison of the 14- and 12-membered ligands shows a significant ring size effect. The smaller ring complexes are generally easier to oxidize, which may be explained simply on the basis of size; the smaller cavity more greatly stabilizes the smaller oxidized metal ion. Conversely, the larger ligands favor the larger lower valent metal ions. Only in the unsubstituted ligands 3 and 4 is this trend reversed. With these ligands, for both the Fe²⁺ and Mn²⁺ complexes, the complex of the larger ligand is slightly easier to oxidize. Here, the unsubstituted ligands may be less rigid than those containing only tertiary N, allowing 3 to more easily adapt to the small Fe³⁺ ion than with the substituted ligands. Ligand 4, because of its small size, should retain more of its rigidity even when unsubstituted, and may not adjust to small Fe³⁺ as well. In spite of the electrochemistry, the overall ability of the ligand 3 to engulf Fe³⁺ is still greater than that of ligand 4 (see discussion of dimer crystal structures above.)

Going from the methyl- to the benzyl-substituted derivatives has only a small effect on the redox potentials. For example the Mn³⁺/Mn²⁺ wave changes from +0.522 V for Mn(5)Cl₂ to +0.577 V in Mn(1)Cl₂. The Fe³⁺/Fe²⁺ wave is similarly changed from +0.110 V for Fe(5)Cl₂ to +0.157 V in Fe(1)Cl₂. Similar effects are observed in the complexes of 4 as compared to those of 6. Comparison of the methyl-substituted and the unsubstituted ligands shows substantial changes. The Mn³⁺/Mn²⁺ wave changes from +0.522 V for Mn(5)Cl₂ to +0.239 V in Mn(3)Cl₂. The Fe³⁺/Fe²⁺ wave is also substantially changed from +0.110 V for Fe(5)Cl₂ to –0.113 V in Fe(3)Cl₂. This effect is lessened in the complexes of 4 and 6, where the Mn³⁺/Mn²⁺ wave changes only from +0.466 V for Mn(6)Cl₂ to +0.389 V in Mn(4)Cl₂, and the Fe³⁺/Fe²⁺ potential, only from +0.036 V for Fe(6)Cl₂ to –0.055 V in Fe(4)Cl₂. Again, large changes in the flexibility between the substituted and unsubstituted versions of the cyclam-derived ligands might explain the large difference in their redox potentials. The smaller 12N4 derived com-

plexes are still relatively rigid regardless of substitution, and thus their redox potentials are less modified, in the unsubstituted complexes.

4. Conclusions

Fe^{II} and Mn^{II}, as noted in Section 1, are enormously important biological ions. However, their properties have made them difficult to control in oxygenated aqueous systems without the protection of the bulky, hydrophobic proteins provided by nature. The ligands 1–6 are designed to produce Mn²⁺ and Fe²⁺ complexes that are stable in aqueous solutions, and under other harsh conditions, to take advantage of their known catalytic reactivities. Here, we have reported the synthesis of Mn²⁺ and Fe²⁺ complexes of the cross-bridged macrobicyclic ligands 1–4, overcoming their proton-sponge nature by reducing the activity of protons in the reaction mixture, following the lead provided in work with ligands 5–6. The derivatives of the larger rings display more positive oxidation potentials, which can be traced to a better size match between the larger ring and the larger lower valent ions and the smaller rings with the smaller higher valent ions. The potentials of the complexes of the present ligand 1–4 complexes are not greatly changed from those of the previously characterized complexes of ligands 5–6. It is therefore expected that they will not have vastly different aqueous reactivities. The new complexes also suffer the disadvantage of being only sparingly soluble in water. These factors combine to suggest that further studies on the catalytic behavior of this class of complexes are best reserved for the parent, methyl-substituted complexes, until other derivatives of greater solubility and more perturbed electrochemistry are designed and synthesized.

5. Supporting information available

Tables of bond distances and angles, atomic coordinates, anisotropic displacement parameters, and isotropic displacement parameters for Mn(1)(CF₃SO₃)₂, Mn(2)Cl₂, Fe(2)Cl₂, [Cl(3)Fe(μ-O)Fe(3)Cl]Cl₂·H₂O, and [Cl(4)Fe(μ-O)Fe(4)Cl]Cl₂·2H₂O are available from the authors upon request.

Acknowledgements

The funding of this research by the Procter and Gamble Company is gratefully acknowledged. T.J.H. thanks the Madison and Lila Self Graduate Research Fellowship of the University of Kansas for financial support. We thank EPSRC and Siemens Analytical Instruments for grants in support of the diffractometer.

The Kansas/Warwick collaboration has been supported by NATO.

References

- [1] F.A. Cotton, G. Wilkinson, *Advanced Inorganic Chemistry*, 5th ed., Wiley, New York, 1988.
- [2] P.R. Ortiz de Montellano (Ed.), *Cytochrome P450: Structure, Mechanism, and Biochemistry*, Plenum Press, New York, 1986.
- [3] (a) H.G. Jang, D.D. Cox, L. Que, Jr., *J. Am. Chem. Soc.* 113 (1991) 9200;
(b) S. Han, L.D. Eltis, K.N. Timmis, S.W. Muchmore, J.T. Bolin, *Science* 270 (1995) 976.
- [4] (a) B.J. Waller, J.D. Lipscomb, *Chem. Rev.* 96 (1996) 2625;
(b) A.C. Rosenzweig, P. Nordlund, P.M. Takahara, C.A. Frederich, S. Lippard, *J. Chem. Biol.* 2 (1995) 409;
(c) L. Que, Jr., Y. Dong, *Acc. Chem. Res.* 29 (1996) 190.
- [5] J.C. Boyington, B.J. Gaffney, L.M. Amzel, *Science* 260 (1993) 1482.
- [6] (a) V.L. Pecoraro (Ed.), *Manganese Redox Enzymes*, VCH, New York, 1992;
(b) B.K. Vainshtein, W.R. Melik-Adayamyan, V.V. Barynin, A.A. Vagin, A.I. Grebenko, *Proc. Int. Symp. Biomol. Struct. Interact., Suppl. J. Biosci.* 8 (1985) 471;
(c) V.V. Barynin, A.A. Vagin, W.R. Melik-Adayamyan, A.I. Grebenko, S.V. Khangulov, A.N. Popov, M.E. Andrianova, B.K. Vainshtein, *Dokl. Akad. Nauk, SSSR* 228 (1986) 877;
(d) K. Weighardt, *Angew. Chem., Int. Ed. Engl.* 28 (1989) 1153.
- [7] (a) M.L. Ludwig, A.L. Metzger, K.A. Patridge, W.C. Stallings, *J. Mol. Biol.* 219 (1991) 335;
(b) G.E.O. Borgstahl, H.E. Parge, M.J. Hickey, W.F. Beyer, Jr., R.A. Hallewell, J.A. Tainer, *Cell* 71 (1992) 107.
- [8] (a) D.M. Prosperpio, R. Hoffman, G.C. Dismukes, *J. Am. Chem. Soc.* 114 (1992) 4374;
(b) T. Ono, T. Noguchi, Y. Inoue, M. Kusunoki, T. Matsushita, H. Oyanagi, *Science* 258 (1992) 1335;
(c) U. Bossek, T. Weyhermüller, K. Weighardt, B. Nuber, J. Weiss, *J. Am. Chem. Soc.* 112 (1990) 6387.
- [9] (a) K. Wieghardt, U. Bossek, B. Nuber, J. Weiss, J. Bonvoisin, M. Corbella, S.E. Vitols, J.J. Girerd, *J. Am. Chem. Soc.* 110 (1988) 7398;
(b) V.C. Quee-Smith, L. DelPizzo, S.H. Jurellar, J.L. Kershner, R. Hage, *Inorg. Chem.* 35 (1996) 6461;
(c) J.H. Koek, S.W. Russel, L. van der Wolf, R. Hage, J.B. Warnaar, A.L. Spek, J. Kershner, L. DelPizzo, *J. Chem. Soc., Dalton. Trans.* (1996) 353;
(d) D.E. De Vos, T. Bein, *J. Organomet. Chem.* 520 (1996) 195.
- [10] D.H. Busch, *Chem. Rev.* 93 (1993) 847.
- [11] (a) G.R. Weisman, M.E. Rogers, E.H. Wong, J.P. Jasinski, E.S. Paight, *J. Am. Chem. Soc.* 112 (1990) 8604;
(b) A. Bencini, A. Bianchi, C. Bazzicalupi, M. Ciampolini, V. Fusi, M. Micheloni, N. Nardi, P. Paoli, B. Valtancoli, *Supramol. Chem.* 3 (1994) 41.
- [12] T.J. Hubin, J.M. McCormick, S.R. Collinson, N.W. Alcock, D.H. Busch, *J. Chem. Soc., Chem. Commun.* (1998) 1675.
- [13] T.J. Hubin, J.M. McCormick, S.R. Collinson, M. Buchalova, C.M. Perkins, N.W. Alcock, P.K. Kahol, A. Raghunathan, D.H. Busch, *J. Am. Chem. Soc.* 122 (2000) 2512.
- [14] T.J. Hubin, J.M. McCormick, N.W. Alcock, D.H. Busch, *Inorg. Chem.* 40 (2001) 435.
- [15] (a) D.H. Busch, S.R. Collinson, T.J. Hubin, *Catalysts and Methods for Catalytic Oxidation*, WO 98/39098, September 11, 1998;
(b) D.H. Busch, S.R. Collinson, T.J. Hubin, R. Labeque, B.K. Williams, J.P. Johnston, D.J. Kitko, J.C.T.R. Burkett-St. Laurent, C.M. Perkins, *Bleach Compositions*, US Patent 6,218,351 B1.
- [16] G.R. Weisman, E.H. Wong, D.C. Hill, M.E. Rogers, D.P. Reed, J.C. Calabrese, *J. Chem. Soc., Chem. Commun.* (1996) 947.
- [17] D.D. Perrin, W.L.F. Armarego, D.R. Perrin, *Purification of Laboratory Chemicals*, 2nd ed., Pergamon Press, New York, 1980.
- [18] E.K. Barefield, F. Wagner, A.W. Herlinger, A.R. Dahl, *Inorg. Synth.* 16 (1976) 220.
- [19] P.S. Bryan, J.C. Dabrowiak, *Inorg. Chem.* 2 (1975) 296.
- [20] H.T. Witteveen, B. Nieuwenhijse, J. Reedijk, *J. Inorg. Nucl. Chem.* 36 (1974) 1535.
- [21] SMART User's Manual, Siemens Industrial Automation Inc., Madison, WI, USA.
- [22] J. Cosier, A.M. Glazer, *J. Appl. Crystallogr.* 19 (1986) 105.
- [23] G.M. Sheldrick, *Acta Crystallogr., A* 46 (1990) 467.
- [24] G.M. Sheldrick, *SHELX-96 (beta-test) (including SHELXS and SHELXL)*, University of Göttingen, Göttingen, Germany, 1996.
- [25] H. Irving, R.J.P.J. Williams, *Chem. Soc.* (1953) 3192 (Part III).
- [26] V.L. Goedken, D.H. Busch, *J. Am. Chem. Soc.* 94 (1972) 7355.
- [27] K.S. Murray, *Coord. Chem. Rev.* 12 (1974) 1.
- [28] (a) P.A. Goodson, D.J. Hodgson, J. Glerup, K. Michelson, H. Weihe, *Inorg. Chem. Acta* 197 (1992) 141;
(b) P.A. Goodson, J. Glerup, D.J. Hodgson, K. Michelson, H. Weihe, *Inorg. Chem.* 30 (1991) 4909;
(c) P.A. Goodson, J. Glerup, D.J. Hodgson, K. Michelson, E. Pederson, *Inorg. Chem.* 29 (1990) 503;
(d) A.R. Oki, J. Glerup, D.J. Hodgson, *Inorg. Chem.* 29 (1990) 2435;
(e) K.J. Brewer, M. Calvin, R.S. Lumpkin, J.W. Otvos, L.O. Spreer, *Inorg. Chem.* 28 (1989) 4446;
(f) K.S. Hagen, W.H. Armstrong, H. Hope, *Inorg. Chem.* 27 (1988) 267;
(g) S.R. Cooper, G.C. Dismukes, M.R. Klein, M. Calvin, *J. Am. Chem. Soc.* 100 (1978) 7248;
(h) P.M. Plaksin, R.C. Stoufer, M. Mathew, G.J. Palenik, *J. Am. Chem. Soc.* 94 (1972) 2121.
- [29] (a) K.J. Brewer, M. Calvin, R.S. Lumpkin, J.W. Otvos, L.O. Spreer, *Inorg. Chem.* 28 (1989) 4446;
(b) C.-M. Che, S.-S. Kwong, C.-K. Poon, T.-F. Lai, T.C.W. Mak, *Inorg. Chem.* 24 (1985) 1359;
(c) C.-K. Poon, C.-M. Che, *J. Chem. Soc., Dalton. Trans.* (1981) 1336;
(d) T.-F. Lai, C.-K. Poon, *Inorg. Chem.* 15 (1976) 1562.
- [30] C.A. Hunter, J.K.M. Sanders, *J. Am. Chem. Soc.* 112 (1990) 5525.
- [31] F.H. Allen, O. Kennard, D.G. Watson, L. Brammer, A.G. Orpen, R. Taylor, *J. Chem. Soc., Perkin Trans. II* (1987) S1.